bioRxiv preprint doi: https://doi.org/10.1101/453423; this version posted February 11, 2019. The copyright holder for this preprint (which was not certified by peer review) is the author/funder. All rights reserved. No reuse allowed without permission.

Unravelling intra- and intersegmental neuronal connectivity between central pattern generating networks in a multi-legged locomotor system

Silvia Daun[1,3], Charalampos Mantziaris[2], Tibor I. Tóth[1], Ansgar Büschges[2], Nils Rosjat[1,3*]

1 University of Cologne, Heisenberg Research Group of Computational Neuroscience - Modelling Neural Network Function, Institute of Zoology, Cologne, Germany

2 University of Cologne, Department of Animal Physiology, Institute of Zoology, Cologne, Germany

3 Research Center Jülich, Institute of Neuroscience and Medicine (INM-3), Jülich, Germany

* n.rosjat@fz-juelich.de

Abstract

Animal walking results from a complex interplay of central pattern generating networks (CPGs), local sensory signals expressing position, velocity and forces generated in the legs, and coordinating signals between neighboring ones. In the stick insect, in particular, intra- and intersegmental coordination is conveyed by these sensory signals. The rhythmic activity of the CPGs, hence of the legs, can be modified by the aforementioned sensory signals. However, the precise nature of the interaction between the CPGs and these sensory signals has remained largely unknown. Experimental methods aiming at finding out details of these interactions, often apply the muscarinic acetylcholine receptor agonist, pilocarpine in order to induce rhythmic activity in the CPGs, hence in the motoneurons of the segmental ganglia. Using this general approach, we removed the influence of sensory signals and investigated the putative connections between CPGs associated with the coxa-trochanter (CTr)-joint in the different segments (legs) in more detail. The experimental data underwent phase-difference analysis and Dynamic Causal Modelling (DCM). These methods can uncover the underlying coupling structure and strength between pairs of segmental ganglia (CPGs). We set up different coupling schemes (models) for DCM and compared them using Bayesian Model Selection (BMS). Models with contralateral connections in each segment and ipsilateral connections on both sides, as well as the coupling from the meta- to the ipsilateral prothoracic ganglion were preferred by BMS to all other types of models tested. Moreover, the intrasegmental coupling strength in the mesothoracic ganglion was the strongest and most stable in all three ganglia.

bioRxiv preprint doi: https://doi.org/10.1101/453423; this version posted February 11, 2019. The copyright holder for this preprint (which was not certified by peer review) is the author/funder. All rights reserved. No reuse allowed without permission.

Keywords

Dynamic causal modelling · Bayesian model selection · Phase-coupling · Stick insect · Thoracic ganglia

Introduction

Various experiments on vertebrates and invertebrates confirm the existence of central pattern generating networks (CPGs). These networks are responsible for the generation of periodic muscle activity in a given leg [14, 29]. The movement of each leg has to be coordinated with that of the other legs in order to produce walking. In the stick insect *Carausius morosus*, each leg is individually controlled by its own CPGs located in the pro- (front legs), meso- (middle legs) and metathoracic ganglion (hind legs) [15, 46]. Each leg consists of three main leg joints about which leg segments execute coordinated movements during walking and climbing. The thorax-coxa (ThC) joint is responsible for forward and backward movements, the coxa-trochanter (CTr) joint enables the femur to move in upward and downward direction. The femur-tibia (FTi) joint brings about flexing and stretching of the leg by moving the tibia relative to the femur. Each of the leg joints is associated with an antagonistic muscle pair: the protractor-retractor (ThC), the levator-depressor (CTr) and the flexor-extensor (FTi) muscle pair [19]. The rhythmic (periodic) activation of the muscles originates in the corresponding CPGs [5]. The coordinated motor output between them, both intrasegmentally and intersegmentally is brought about by sensory signals [2–4, 21, 25]. In addition, a previous study showed that, in the absence of sensory feedback, depressor CPG activity is weakly coupled to the one of all other segments [28]. The authors demonstrated that the different intrasegmental phase relationships for isolated ganglia were stabilized in the case of interconnected ganglia. However, little is known about the interaction, i.e. the strength and the nature of the couplings between the different CPG networks. In order to understand how a stable locomotor pattern is generated, we need to understand the contribution of the central and peripheral sensory signals, and the interactions between them. Up to now, there has been a long and successful history of mathematically describing and modelling central pattern generating networks by means of phase oscillators [10]. A variety of interesting and fruitful insights have been gained from the models of weakly coupled oscillators [9, 27, 37]. Nevertheless, there is a drawback of this modelling approach. Hitherto, no method has been found to estimate the coupling strengths *from the data* and not from the model itself. Meaning that in the stick insect in particular, the connection strengths between the various CPGs in the different ganglia has not been studied (to the best of our knowledge also not for other insects at least not for the whole nerve cord).

bioRxiv preprint doi: https://doi.org/10.1101/453423; this version posted February 11, 2019. The copyright holder for this preprint (which was not certified by peer review) is the author/funder. All rights reserved. No reuse allowed without permission.

There are some promising approaches though concerning electroencephalography (EEG) and magnetoencephalography (MEG) recordings, e.g. [23, 33]. In this paper, we aim at tackling the problem of estimating the coupling strength by using two different methods. The first one is simple and essentially descriptive. The second one is a more complex, modelling approach. Both serve the purpose of assigning relative coupling strengths to the (neuronal) connections between the levator-depressor CPGs in different hemisegments.

Usually, the interaction between oscillators is characterized by the coupling strengths between them. These coupling strengths, as a matter of course, originate from a model that was somehow fitted to the data, e.g. [35]. As there is no direct relation between the recorded data and the model parameters, we decided to investigate the effect of central coupling from both directions. Starting from the data analysis, we used the descriptive method, while starting from modelling, we endeavored to obtain reasonable estimates on the strength of the coupling between the CPGs of the different segments in the thoracic nerve cord.

This article is organized as follows: in the section 1 *Materials and methods*, we will first review the experimental methods and explain the basic properties of the phase-difference approach and the Dynamic Causal Modelling (DCM) including Bayesian Model Selection (BMS), which we use for the data analysis in the present work. The section 2 *Results* is divided into three parts. In the first part, we will present the results of the analysis for the meso- and metathoracic ganglia, in the second part, the results for the pro- and mesothoracic ganglia, and in the third part, we will show the results for the combined analysis of the pro-, meso- and metathoracic ganglia. Finally, the sections 3 *Discussion* and 4 *Conclusion* will follow.

1 Materials and methods

Animals

The experiments were carried out on adult female Indian stick insects of the species *Carausius morosus* [45]. The animals are obtained from the colony at the University of Cologne maintained at 22-24°C, at approximately 60% humidity and under a 12 h light / 12 h dark cycle.

Preparation

We extracellularly recorded the rhythmic activity from C2 leg nerves, which contain the axons that innervate the slow and the fast *depressor trochanteris* muscles (SDTr and FDTr respectively) [39]. We did so with the nerves in the contralateral pro-, meso- and metathoracic ganglia using 'hook' electrodes [40].

bioRxiv preprint doi: https://doi.org/10.1101/453423; this version posted February 11, 2019. The copyright holder for this preprint (which was not certified by peer review) is the author/funder. All rights reserved. No reuse allowed without permission.

To this end, all legs of the stick insects were removed, all lateral and connective nerves, except the ones of interest, were cut off (isolated and deafferented preparation). Also axons of sensory neurons were destroyed to prevent sensory feedback and peripheral input from being recorded. Rhythmic activity in leg motoneuron (MN) pools was then induced by bath application of $5-7$ mM of the muscarinic receptor agonist *pilocarpine* [5]. For a detailed description of the preparation, experimental setup and electrophysiology see [28].

Data preprocessing

The collected data were preprocessed offline using Spike2 7.09 (CED, Cambridge, UK). We used the signal processing functions DC-remove, Rectify and Smooth to get rectified and smoothed waveforms that are corrected for DC (direct current) shifts, i.e. having a mean amplitude of zero. These data were then downsampled to 200 Hz, extracted as a time-series.

Connectivity analysis

The data was further processed with MatLab R2011b (The MathWorks Inc., Massachusetts, USA) and Python 2.7.14. Phase-difference analysis was done using custom programmed MatLab scripts and clustering algorithms implemented in the Python toolbox sci-kit learn [34]. For Dynamic Causal Modelling (DCM), we used the Statistical Parametric Mapping toolbox (SPM12, Wellcome Trust Centre for Neuroimaging, London, UK) implemented in MatLab.

Phase-connectivity approach (PC)

We analyzed, *in the absence of sensory input*, the coordination of the rhythmic motor activities in the stick insect in order to uncover possible phase-coupling between them. The analysis was performed by means of established methods that are described elsewhere [37,43]. Using this approach, we gained information of the time evolution of multiple rhythms propagating intra- or intersegmentally. The intersegmental analysis was done for the meso- and metathoracic ganglia first and then for the pro- and mesothoracic ganglia. We analyzed the phase of the neural activity in each nerve as the activity evolved in time. For automatic and objective detection of burst onsets the preprocessed extracellular recordings were used to construct a discrete-time analytic signal

$$X = X_r + iX_i, \tag{1}$$

bioRxiv preprint doi: https://doi.org/10.1101/453423; this version posted February 11, 2019. The copyright holder for this preprint (which was not certified by peer review) is the author/funder. All rights reserved. No reuse allowed without permission.

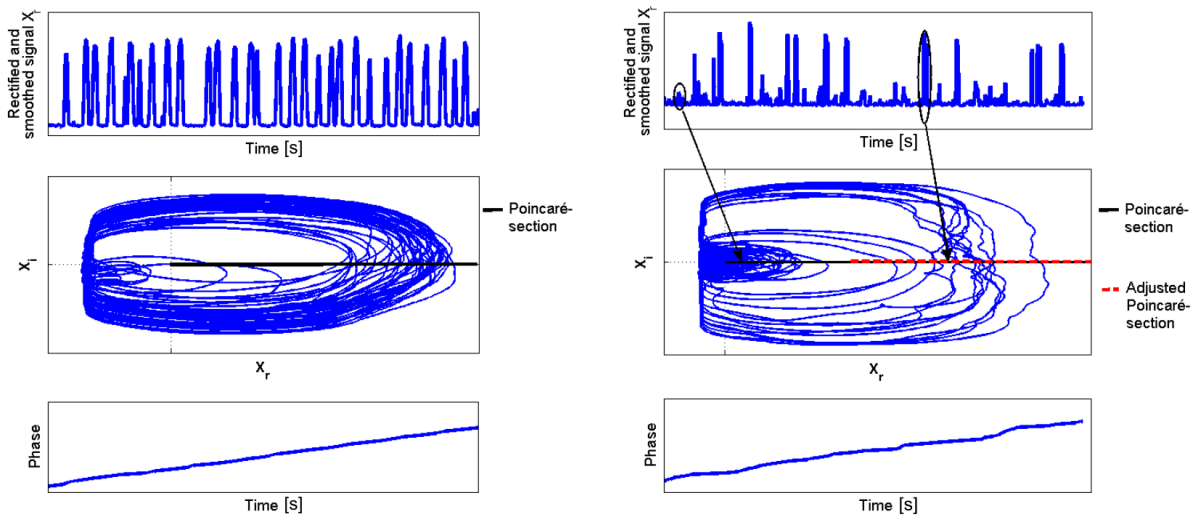

Fig 1. Top: Rectified and smoothed signal X_r (Left: meso-meta, Right: pro-meso); Middle: Discrete-time analytic signal with Poincaré-section marked in black (normal) and red (adjusted for small units) (Left: meso-meta, Right: pro-meso); Bottom: Resulting instantaneous (unwrapped) phase φ (Left: meso-meta, Right: pro-meso).

in the complex plane. Here, X_r is the real data vector, and X_i is the Hilbert transform of X_r [30]. Then a Poincaré-section was used to define the onsets of the bursts and thereby the reference phase of the rhythm. To obtain information on the phase φ of each recording, we linearly interpolated the phase angle between each pair of onsets and normalized it to lie in the interval $[0, 1)$ (mod 2π) during one cycle. As a last step, the phase was unwrapped, i.e. it grew monotonically, as if it were an 'ordinary' non periodic time signal (Fig 1, left). When recording from the prothoracic ganglion, the signals showed activities with small amplitudes, in addition to the large amplitude bursts. Thus, we modified the analysis by adjusting the Poincaré-section such that only the big amplitudes were marked as burst onsets (Fig 1, right; second black circle in the top panel). The adjustment was based on the k-means clustering algorithm implemented in the sci-kit learn toolbox in Python [26, 34] for k=2. This method optimizes two centroids representing the small and big amplitude peaks and then assigns each detected peak to the closest cluster.

To investigate the coupling of two CPGs, we calculated their phase-difference. The signals are considered to be coupled if their phase-difference remains constant over a certain time-period, i.e.

$$||\varphi_1(t) - \varphi_2(t)|| = c + \varepsilon, \tag{2}$$

ε being a small error (compared to c). In our analysis, we ensured this by requiring the following two criteria to be fulfilled for the R-vector (cf. [1]), which measures the similarity of the phase-differences of the coupled phases ranging from 0 (random phase-differences) to 1 (identical phase-differences):

bioRxiv preprint doi: https://doi.org/10.1101/453423; this version posted February 11, 2019. The copyright holder for this preprint (which was not certified by peer review) is the author/funder. All rights reserved. No reuse allowed without permission.

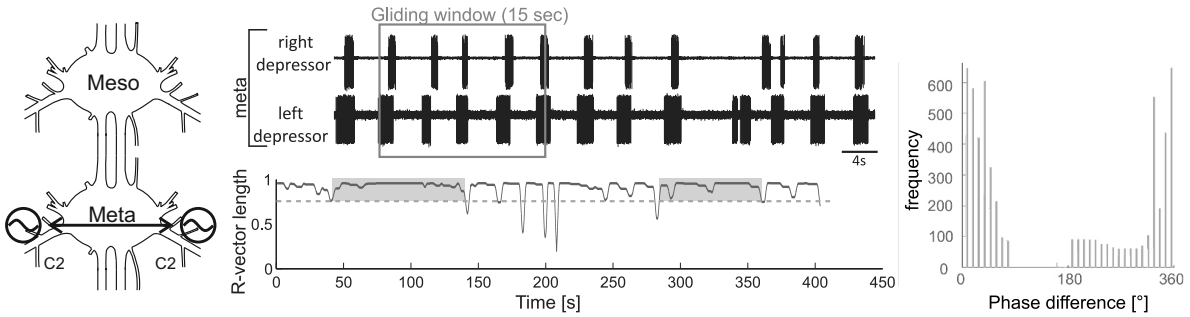

Fig 2. Left: Schematic drawing showing which segmental depressor activity has been recorded and analyzed. Middle top: Sample recording of left and right depressor activity in the metathoracic ganglion; Middle bottom: Development of the R-vector length of left-right metathoracic phase-differences over a whole recording, coupled intervals are marked with grey boxes; Right: Phase-histogram shown for the coupled interval $\approx$ [50,140] (see text for details).

1. The length of the R-vector in a 15 s long gliding time-window should be larger than 0.8 for at least 50 s (corresponds to 10 cycles) (Fig 2, lower panel in the middle).

2. Over the whole time-interval defined in 1., there should be a clear peak in the histogram (Fig 2, right), with a R-vector larger than 0.3. This criterion prevents drifting of the phases over the interval where coupling exists.

Both thresholds for the R-vectors were adjusted manually in such a way that the program was able to correctly assign clearly coupled or clearly uncoupled intervals to the correct group. We defined coupling strength to be the likelihood of coupling over the whole recording, i.e. the sum of all interval lengths in which coupling occurred divided by the total length of the corresponding record. Records with no coupling were taken into account with 0 s of coupling.

Dynamic Causal Modelling approach

In the second approach, we made use of Dynamic Causal Modelling (DCM) [23] to investigate the type and strength of intra- and intersegmental coupling between the thoracic ganglia of the levator-depressor system of the stick insect. This approach is widely used in the analysis of couplings in M/EEG and fMRI data [6, 20, 44], and in the analysis of local field potentials [33].

It uses neural mass models [31, 32] to describe the neuronal activity of the recorded sources (in our case CPGs). As there is no stimulation in our experimental setup, *i.e. absence of sensory input*, we selected the DCM for cross-spectral density (CSD) approach that does not include any inputs and is suitable for modelling steady-state like data [16]. This particular DCM approach is based on a linearization of dynamical systems, i.e. neuronal subpopulations are coupled via their mean fields. The connectivity is determined by modeling coherence and phase-differences of the observed electrophysiological measurements. A model is optimized using empirical measures of cross-spectral densities. In particular,

bioRxiv preprint doi: https://doi.org/10.1101/453423; this version posted February 11, 2019. The copyright holder for this preprint (which was not certified by peer review) is the author/funder. All rights reserved. No reuse allowed without permission.

the parameter values are fitted within a system of differential equations according to a predefined coupling structure to model (explain) the recorded source activity:

$$\dot{z} = (A + uB)z, \tag{3}$$

where z is the output activity of the sources. The coupling structure is defined in the matrix A, and possible connectivity changes between different experimental conditions are modelled by using B. The coupling strengths saved in A and B will then be fitted in order that $z(t)$ has, in some well-defined sense, the smallest distance from the recorded activity, i.e. being optimal in that sense.

Statistical Methods

The best coupling structure in the DCM approach is determined by Bayesian Model Selection (BMS) [36]. This method yields two measures: (i) the relative logarithmic model evidence and (ii) the model posterior probability. The logarithmic model evidence $\log B_{ji}$ of a model j is displayed relative to the least probable model i.

$$\log B_{ji} = \log \mathsf{p}(y|m = j) - \log \mathsf{p}(y|m = i), \tag{4}$$

with the probability $\mathsf{p}(y|m = j)$ describing the likelihood of the observed data being generated by model j. Given equal priors $p(m = i) = p(m = j)$ (for the different models) the posterior probability of model i $p(m = i|y)$ is

$$p(m = i|y) = \frac{1}{1 + \exp(-\log(B_{ij}))}. \tag{5}$$

Finding the best coupling structure via BMS enables us to investigate intra- and intersegmental coupling strengths in the preferred model architecture (see Fig 4).

Significant differences in connectivity strengths were in both approaches (PC and DCM) determined by means of t-tests. In the DCM approach we assumed left-right symmetry and thus assigned both directions of a connection between two CPGs to the same connection (e.g. connection strengths from the left mesothoracic to the right mesothoracic and from the right mesothoracic to the left mesothoracic ganglion were averaged). This does not apply to the PC approach, since no directionality of the connections is obtained here.

bioRxiv preprint doi: https://doi.org/10.1101/453423; this version posted February 11, 2019. The copyright holder for this preprint (which was not certified by peer review) is the author/funder. All rights reserved. No reuse allowed without permission.

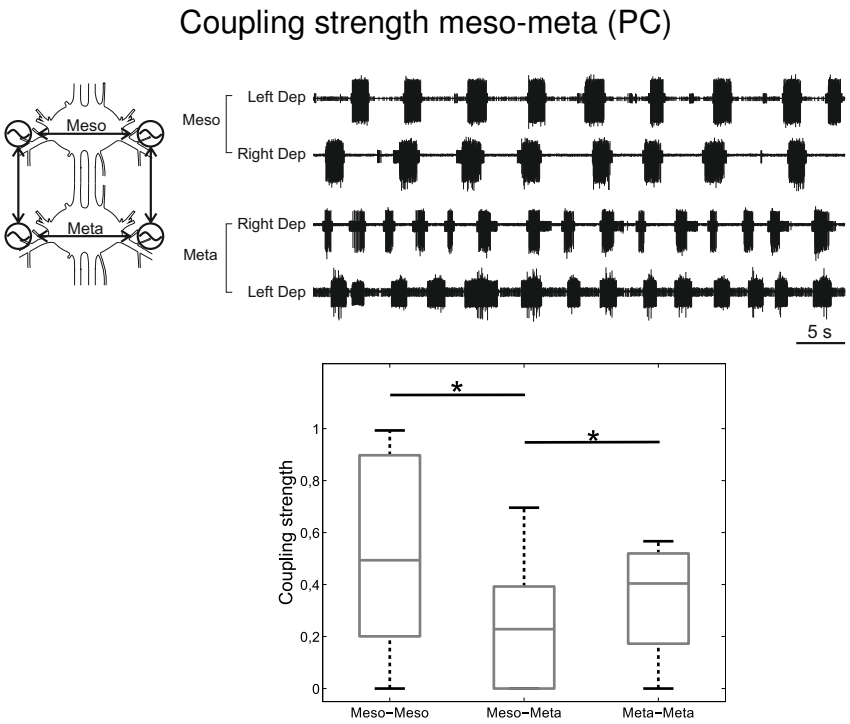

Fig 3. Top: Sample recording of left and right depressor activity in the meso- and metathoracic ganglia; Bottom: Coupling strength in the meso-meta thoracic ganglia over all experiments using the phase-connectivity (PC) approach ($N = 10$). Meso-Meso denotes coupling between both sides of the mesothoracic and meta-meta the one between the both sides of the metathoracic ganglion. Meso-Meta represents the intersegmental coupling between the meso- and the metathoracic ganglia. * denotes statistical significant differences.

2 Results

In this study, we report results obtained with methods commonly used to analyze M/EEG data. We applied them to analyze the coupling strengths of pharmacologically induced rhythmic MN activity of the stick insect. Coupling between the motor systems of the CTr-joints of several segments, such as meso-meta, pro-meso was investigated; first, the phase relations of the bursting activities and then by means of mathematical models that reproduce characteristic properties of the recorded depressor MN activity. Moreover, the models were used to obtain information on the coupling structure of the whole walking system involving all three (pro-, meso-,meta-) thoracic segments.

Meso-Meta thoracic ganglia

In the first part of the experiment, the activity of the contralateral C2 nerves of the meso- and metathoracic ganglia was recorded. Data from both sides in the meso- and metathoracic ganglion were collected in 10 animals.

bioRxiv preprint doi: https://doi.org/10.1101/453423; this version posted February 11, 2019. The copyright holder for this preprint (which was not certified by peer review) is the author/funder. All rights reserved. No reuse allowed without permission.

BMS meso-meta

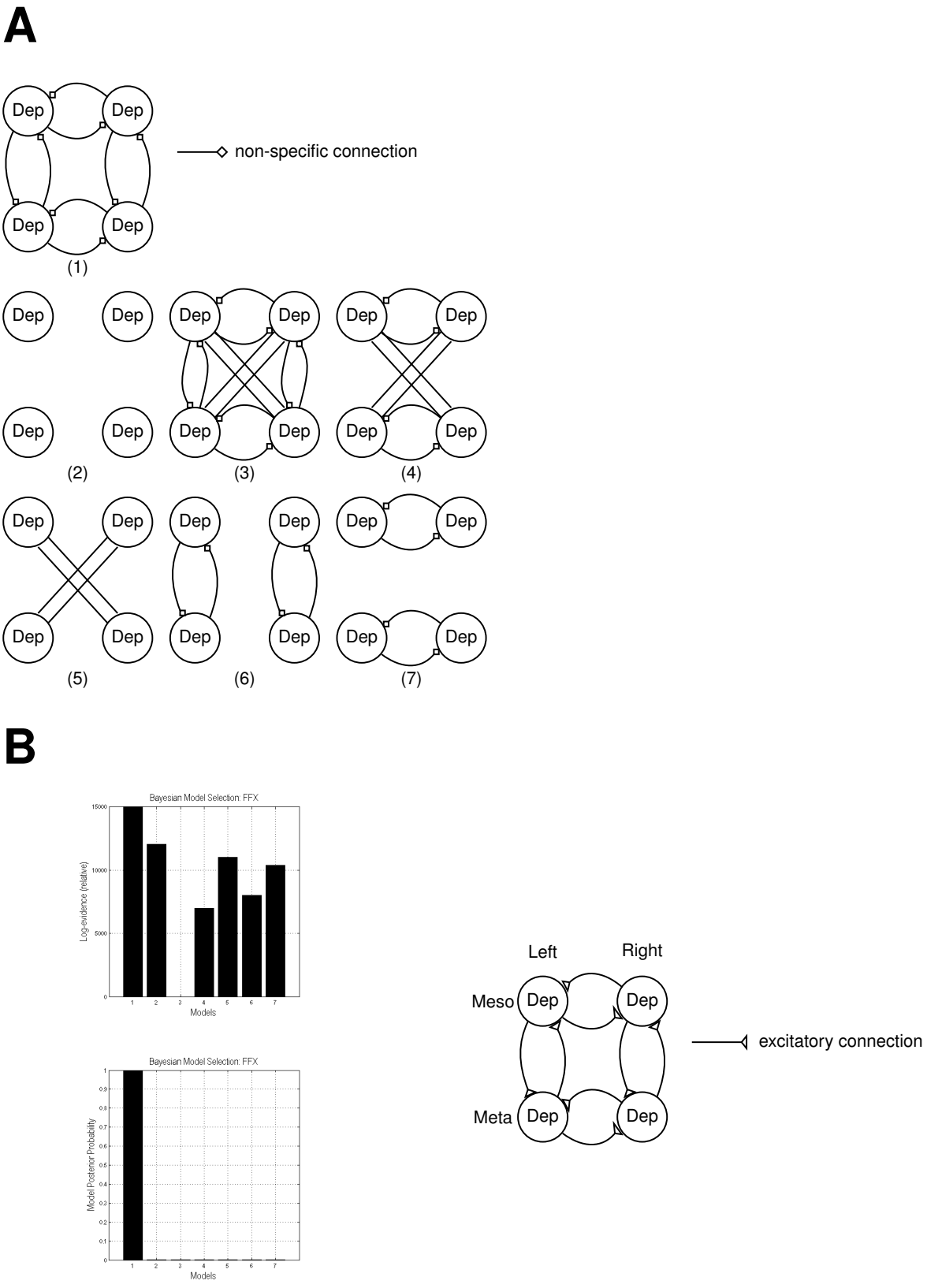

Fig 4. A: Model architectures tested with DCM. B: Model selection (see text for details); Left: Log-evidence and posterior probability of Bayesian Model selection for the meso-meta thoracic ganglia are highest for model (1); Right: Structure of the winning model (1), triangles marking excitatory connections between CPGs.

bioRxiv preprint doi: https://doi.org/10.1101/453423; this version posted February 11, 2019. The copyright holder for this preprint (which was not certified by peer review) is the author/funder. All rights reserved. No reuse allowed without permission.

The results of the phase-coupling (PC) approach are presented in Fig 3. The likelihood was highest for the intrasegmental couplings, i.e. the coupling between both sides of the mesothoracic ganglion (meso-meso) and the coupling between both sides of the metathoracic ganglion (meta-meta). A paired t-test showed that the likelihood of intersegmental coupling (meso-meta) was significantly lower ($p = 0.0396$) than the intrasegmental couplings, while comparison of the intrasegmental couplings of meso-meso and meta-meta types showed no significant difference ($p = 0.2224$) between them.

In the next step, we used the bilaterally recorded data for the DCM analysis. First, we tested a number of possible predefined coupling structures. The models tested consisted of unconnected (2), fully connected (3) ganglia, cross connected ganglia with (4) and without intrasegmental connections (5), ipsilaterally connected ganglia (6), intersegmentally unconnected (7), and circularly connected ganglia (1) (Fig 4 A). All models were tested with excitatory and inhibitory connections. Here, we show the results with excitatory coupling, only, since in both cases (excitatory and inhibitory), the same winning model structure emerged but the winning model with excitatory connections had a higher probability according to the Bayesian Model Selection (BMS) procedure. BMS also showed that model (1) with the circular coupling structure best fitted the recorded data (Fig 4 B, left), since log-evidence and model posterior probability were highest.

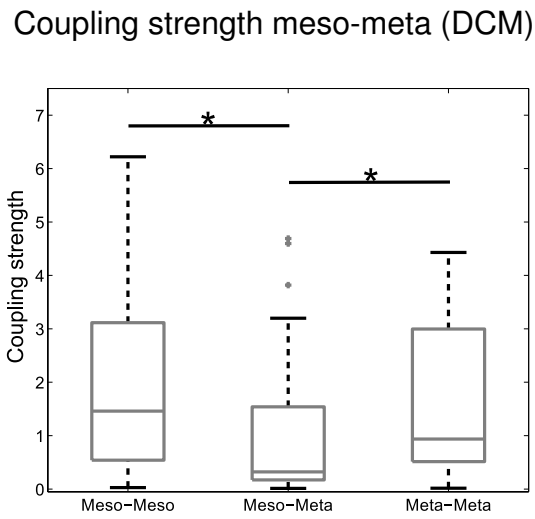

Fig 5. Coupling strength in the meso-meta thoracic ganglia over all experiments using the DCM approach ($N = 5$, $n = 11$) for *biased* intervals already identified as coupled by the phase-coupling approach. Meso-Meso denotes coupling between both sides of the mesothoracic and meta-meta the one between the both sides of the metathoracic ganglion. Meso-Meta represents the intersegmental coupling between the meso- and the metathoracic ganglia. * denotes statistical significant differences.

bioRxiv preprint doi: https://doi.org/10.1101/453423; this version posted February 11, 2019. The copyright holder for this preprint (which was not certified by peer review) is the author/funder. All rights reserved. No reuse allowed without permission.

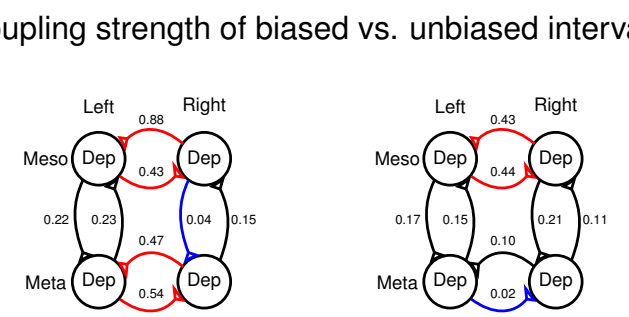

Fig 6. Coupling strength for the same animal. Left: *biased* interval of 50 s length, Right: *unbiased* interval composed of 5 intervals of 15 s length each. The strongest connections are marked with red lines and the weakest connections are marked with blue lines, respectively.

We used this coupling structure as the basis for estimation of the coupling strengths. We decided to analyze the recordings in two steps. First, we used *biased* intervals, i.e. intervals that were identified as coupled in the phase-coupling analysis, then we analyzed *unbiased*, i.e. arbitrary chosen time-intervals. By this, we could gain information on the differences in coupling strengths during phase-synchronized time-intervals in comparison to unsynchronized ones.

The analysis of the *biased* (phase synchronized) intervals yielded the coupling strengths, which are depicted in Fig 5. In agreement with the phase-coupling analysis, we found the strongest coupling in the meso-meso and meta-meta connectivity, while the meso-meta connectivity was significantly weaker (tested with a t-test compared to meso-meso: $p = 0.013$, and compared to meta-meta: $p = 0.041$). Then we looked at five *unbiased*, i.e. arbitrary chosen intervals of 15 s duration each that we merged together into one time interval. The corresponding coupling strengths are displayed in Fig 6, right. When comparing the coupling strengths found in the biased intervals of a particular animal (data from that animal shown in Fig 6, left), we could see that the coupling strengths in the mesothoracic ganglion and the intersegmental coupling strengths stayed roughly the same, while the coupling strengths in the metathoracic ganglion were reduced by a factor of five. The results obtained from the other animals were similar. This suggests that the mesothoracic intrasegmental coupling remains high throughout the whole experiment whereas the coupling in the metathoracic ganglion is strong only in the intervals where phase-coupling between them is also present.

Since DCM was developed for data recorded from the human brain, we tested whether it could reasonably be applied to extracellular nerve recordings from animals. Therefore, we additionally cut the connectives between the meso- and metathoracic ganglia in the experiments. This surgical manipulation completely destroyed the connectivity between the two segments. We originally set up DCM to calculate coupling strengths of the fully connected system (A-matrix). Changes from this (cut connectives) were taken into account in the B-matrix (cf. Eq. 3). We did not provide any prior information on which connections should be changed by DCM. The model showed a strong decrease of the connection

bioRxiv preprint doi: https://doi.org/10.1101/453423; this version posted February 11, 2019. The copyright holder for this preprint (which was not certified by peer review) is the author/funder. All rights reserved. No reuse allowed without permission.

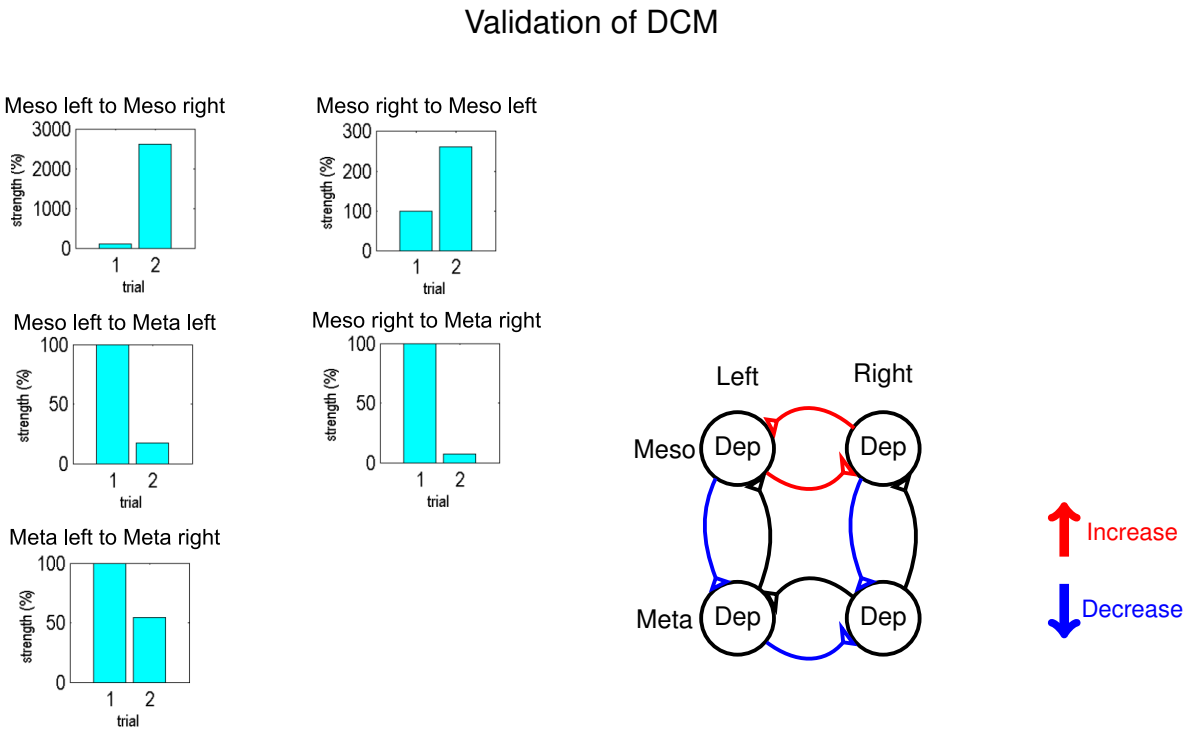

Fig 7. Significant differences in connectivity from meso-meta thoracic connected segments (trial 1) to unconnected segments (trial 2). Left: Changes of connectivity strength, with trial 1 normalized to 100% coupling strength; Right: Changes of connectivity compared to trial 1, red lines mark an increase in connectivity, blue lines a decrease in connectivity and black lines no reliable connectivity change (above 70%).

strength, 90% on the left side and 95% on the right side, between the meso- and metathoracic ganglion (Fig 7). The connection between both segments was not completely removed by DCM. This is due to the fact that DCM is constructed to use a minimal connection strength whenever it is assumed to be present. In addition to the intersegmental decrease, there was a strong increase in the intrasegmental coupling in the mesothoracic ganglion (by factors of 2-20) and a decrease in connectivity in the metathoracic ganglion (by a factor of 2). This is in agreement with [28] where the authors could demonstrate that the mesothoracic ganglion showed intrasegmental phase-coupling even in the isolated state, while the connection of the metathoracic ganglion to the mesothoracic ganglion had to be present to detect robust in-phase coupling in the metathoracic ganglion.

Pro-Meso thoracic ganglia

In the second part, we analyzed the coupling between the pro- and the mesothoracic ganglia. We recorded the activity of the C2 nerve on both sides of both ganglia in 5 animals, on both sides of the mesothoracic ganglion and on one side of the prothoracic ganglion in 3 animals and on both sides of the prothoracic and on one side of the mesothoracic ganglion in 5 animals.

bioRxiv preprint doi: https://doi.org/10.1101/453423; this version posted February 11, 2019. The copyright holder for this preprint (which was not certified by peer review) is the author/funder. All rights reserved. No reuse allowed without permission.

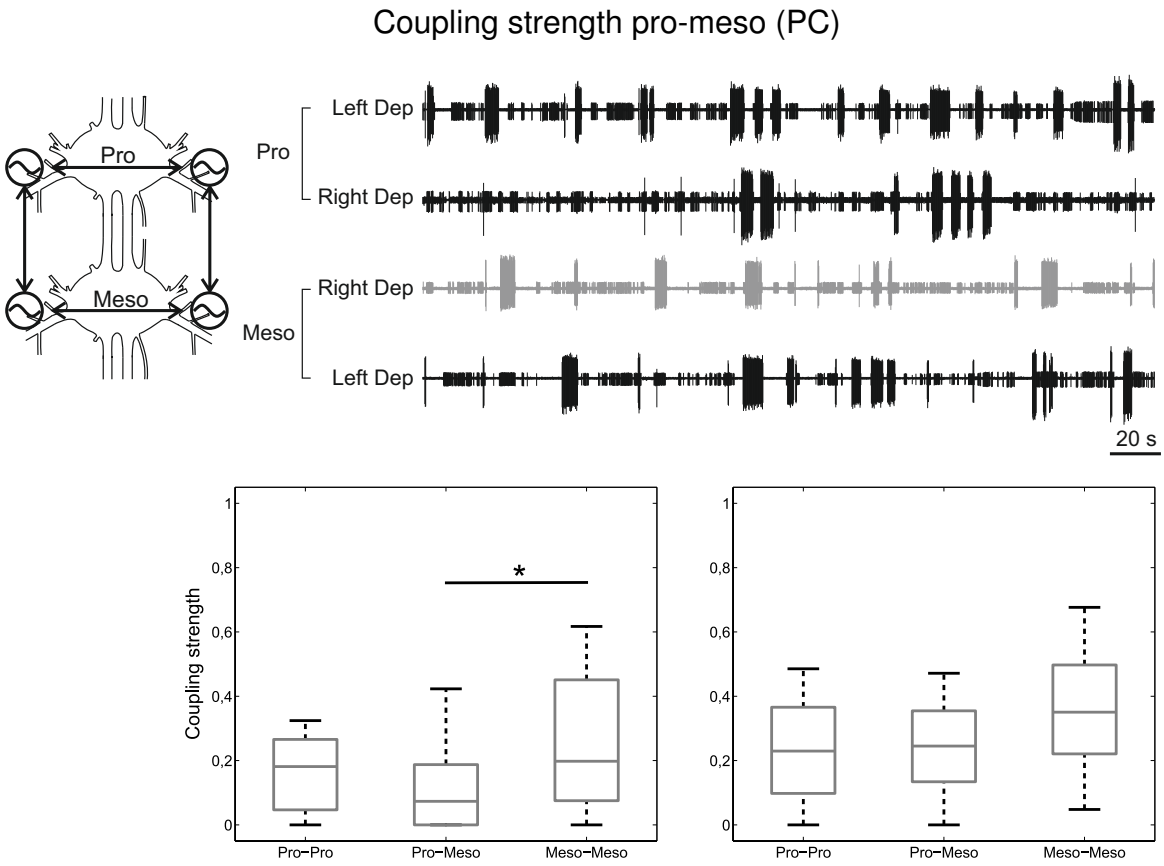

Fig 8. Top: Sample recording of left and right depressor activity in the pro- and mesothoracic ganglia (see scheme on the left); Bottom: Coupling strengths in the pro-meso thoracic ganglia over all experiments using the phase-coupling approach ($N = 13$). Left: without adjustment to the Poincaré-section, Right: With Poincaré-section adjusted to big units. Pro-Pro denotes coupling between both sides of the prothoracic and meso-meso the one between the both sides of the mesothoracic ganglion. Pro-Meso represents the intersegmental coupling between the pro- and the mesothoracic ganglia. * denotes statistical significant differences.

We observed long intervals of tonic SDTr activity, small units in Fig 8, top right, which led to the detection of additional burst onsets by the previously described Poincaré section. Therefore, we now used a modified Poincaré section defined by a semi-automatic clustering method (see Materials and methods) in order to filter out the bursts produced by those units. This basically amounted to applying a higher amplitude threshold to the data (cf. Fig 1, right; adjustment of Poincaré section). Statistical analysis of the PC approach of the non-adjusted phase-differences using t-tests revealed that the intrasegmental coupling in the mesothoracic ganglion was significantly stronger than the intersegmental coupling between the pro- and the mesothoracic ganglion ($p = 0.0394$, Fig 8, bottom left). Additionally, the coupling strength in the mesothoracic ganglion in this experimental condition was significantly reduced compared to the one in the mesothoracic ganglion obtained in the meso-meta recordings ($p = 0.0376$, cf.

bioRxiv preprint doi: https://doi.org/10.1101/453423; this version posted February 11, 2019. The copyright holder for this preprint (which was not certified by peer review) is the author/funder. All rights reserved. No reuse allowed without permission.

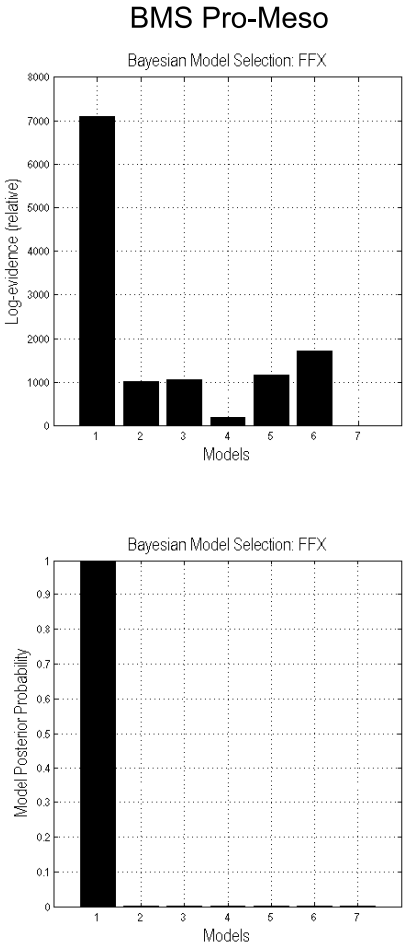

Fig 9. BMS results: Log evidence (top) and posterior probability (bottom) for pro-meso recordings yield model (1) to be the winning model. Models correspond to the ones shown in Fig. 4A.

Fig 3). In the modified analysis, with Poincaré section adjusted to big units, there were no significant differences between all couplings (pp-mm $p = 0.29$, pm-mm $p = 0.541$, pm-pp $p = 0.437$) (Fig 8, bottom right).

We then investigated these data with the DCM approach. The BMS showed the same result as for the meso-meta thoracic ganglia (Fig 9). That is why we used the same coupling structure for the analysis of the coupling strengths in the pro-meso thoracic ganglia (cf. Fig 4 B, right). In the *biased* coupling intervals ($N = 5$, $n = 10$), i.e. in the intervals where a phase coupling was detected a priori by the PC approach, we can see that the intrasegmental meso-meso coupling ($p = 0.003$) and the intersegmental pro-meso coupling ($p = 0.013$) are significantly stronger than the intrasegmental pro-pro coupling as shown by paired t-tests (Fig 10, left). The same pattern can be seen for *unbiased* intervals (Fig 10, right), where we used ten intervals of length of 50 s each that were arbitrarily chosen from five animals. A paired t-test showed that the pro-meso ($p = 0.025$) and meso-meso coupling ($p = 0.001$) were again significantly stronger than the pro-pro coupling.

bioRxiv preprint doi: https://doi.org/10.1101/453423; this version posted February 11, 2019. The copyright holder for this preprint (which was not certified by peer review) is the author/funder. All rights reserved. No reuse allowed without permission.

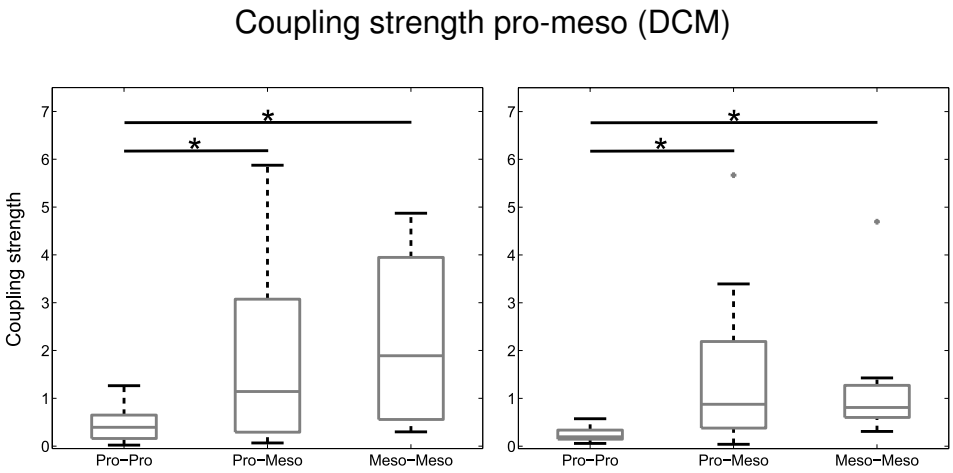

Fig 10. Coupling strengths in the pro-meso thoracic ganglia over all experiments using the DCM approach. Left: Coupling strengths for *biased*, i.e. phase-coupled intervals ($N = 5$, $n = 10$); Right: Coupling strengths for *unbiased*, i.e. arbitrary chosen intervals ($N = 5$, $n = 10$). Pro-Pro denotes coupling between both sides of the prothoracic and meso-meso the one between the both sides of the mesothoracic ganglion. Pro-Meso represents the intersegmental coupling between the pro- and the mesothoracic ganglia. * denotes statistical significant differences.

Pro-Meso-Meta thoracic ganglia

For the analysis of coupling between the pro-, meso- and metathoracic ganglia, we recorded the activity of the C2 nerve on both sides of all three ganglia in 3 animals. Due to the small sample size, it was not possible to analyze the phase-coupling statistically in this data set. We, therefore, focused our analysis on the structure of the combined networks, i.e. pro-meso and meso-meta. Because the cycles could not be clearly defined due to the high variability of SDTr activity (see Fig 11 A, right), we refrained from using the PC approach as a proxy for coupled intervals and used a gliding window of 50 s duration to select five intervals for each animal instead. The models tested with BMS consisted of a union of the previously discussed networks (1), with added cross connections (2), as well as bi- (3) and unidirectional lateral connections (4) between pro- and metathoracic ganglia (Fig 11 B). Model 4 became the winning model (Fig 11 C). Thus, the full network consists of the union of the subnetworks and a lateral feedback from meta- to prothoracic ganglia (Fig 12 B). An a posteriori t-test on the coupling strengths revealed no significant difference between the nine connections (all p's > 0.05). A further t-test on the meso-meso coupling strengths in meso-meta and pro-meso-meta recordings revealed a significantly reduced connectivity in the latter recordings ($p = 0.0044$).

bioRxiv preprint doi: https://doi.org/10.1101/453423; this version posted February 11, 2019. The copyright holder for this preprint (which was not certified by peer review) is the author/funder. All rights reserved. No reuse allowed without permission.

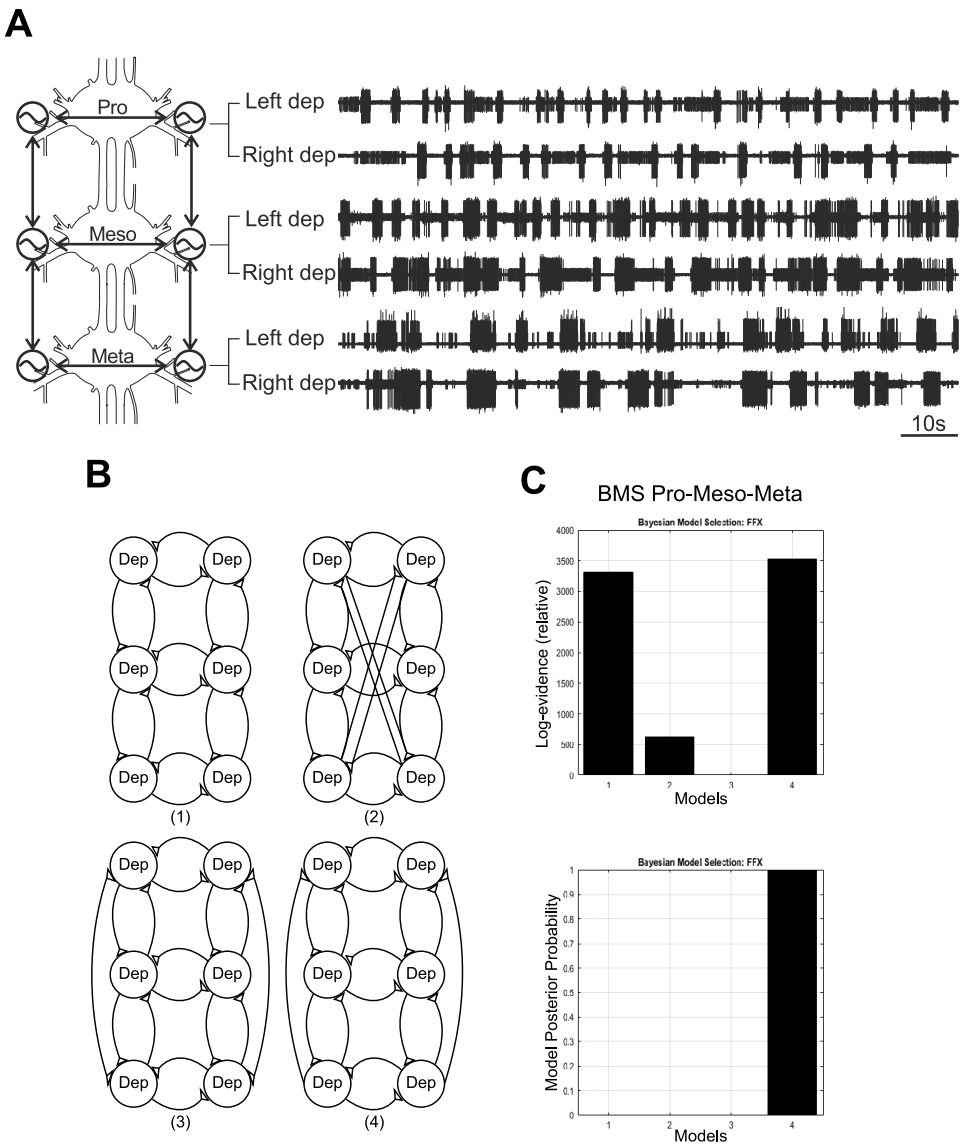

Fig 11. A: Sample recording of left and right depressor activity in the pro-, meso- and metathoracic ganglia (see scheme on the left); B: Different coupling structures tested with BMS. Triangles denote excitatory connections; C: BMS results: Log evidence (top) and posterior probability (bottom) for pro-meso-meta recordings are highest for model (4).

3 Discussion

General coupling structure of CPG networks

In this paper, we, for the first time, provide results on the coupling structure (using DCM) and the coupling strengths (using the DCM and PC approaches) for the whole thoracic nerve cord in a multi-legged, deafferented locomotor system. Our results provide strong evidence that in all animals investigated, the inter- and intrasegmental central couplings follow the same organizational principle. In Fig 12, we sum up the structure and the strengths of the network connectivity from both approaches. BMS on the

bioRxiv preprint doi: https://doi.org/10.1101/453423; this version posted February 11, 2019. The copyright holder for this preprint (which was not certified by peer review) is the author/funder. All rights reserved. No reuse allowed without permission.

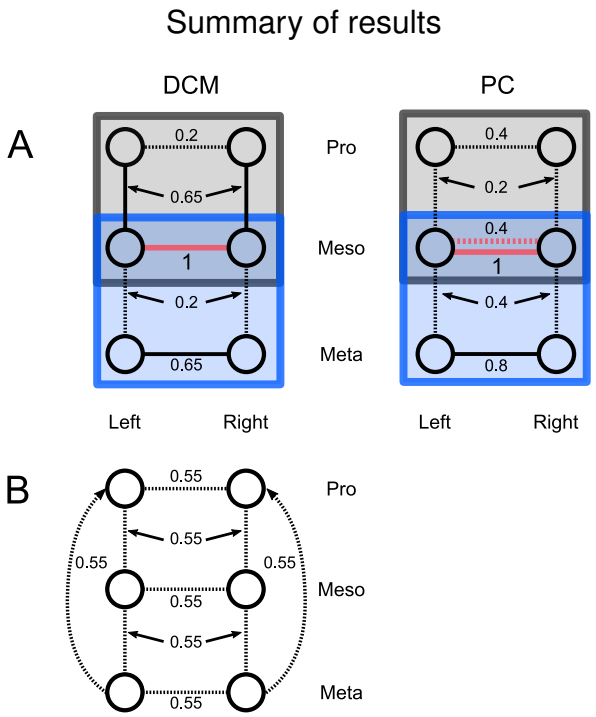

Fig 12. Summary of the coupling strengths (numbers) obtained by the DCM approach (left) and the phase coupling (PC) approach (right). Lines represent the mean of the bidirectional couplings assuming left-right symmetry. A: Recordings involving two ganglia: pro-meso recordings marked by a gray rectangle and meso-meta recordings with a blue rectangle, respectively. B: Recordings involving pro-, meso- and metathoracic ganglia. All coupling strengths are normalized to the meso-meso connectivity (marked with magenta lines) strength in the corresponding meso-meta recordings (blue rectangle). Significantly smaller connectivity strengths are represented by dashed lines.

set of various fitted DCM models preferred an eight-shaped structure consisting of ipsilateral inter- and lateral intrasegmental connections of the CPGs and thus predicted a high probability for the existence of these connections. Importantly, the models containing cross connections, e.g. from pro-left to meso-right, models with missing inter- or intrasegmental coupling and fully connected models were not selected by BMS. The coupling structure we propose here is in accordance with previous results showing that ipsilateral leg coordinating influences are indeed transmitted by the ipsilateral connective [8, 13, 24]. In the following, we will discuss the differences in coupling strengths among the different connections.

Central intersegmental CPG interactions in other locomotor systems

Central intersegmental CPG interactions have been demonstrated in the past using various animal models. In-phase intersegmental activity of MN pools has been reported earlier for deafferented preparations of the crayfish [41] and the stick insect [5] after pharmacological CPG activation. In the deafferented thoracic ganglia of the locust, intersegmental depressor MN activity also expressed similar behavior [24]. In contrast, older data had suggested ipsilateral coupling between ipsilateral levator and depressor MN activity in adjacent ganglia of the locust [38]. In the deafferented thoracic nerve cord of the hawk

bioRxiv preprint doi: https://doi.org/10.1101/453423; this version posted February 11, 2019. The copyright holder for this preprint (which was not certified by peer review) is the author/funder. All rights reserved. No reuse allowed without permission.

moth, pharmacological activation of the depressor MN pools produced an activity pattern that resembled the tripod leg coordination pattern emerging during walking in a large number of insect species [22]. Finally, similar intersegmental coordination patterns were recorded in the interconnected meso- and metathoracic ganglia of the cockroach thoracic nerve cord with the sub-esophageal ganglion (SEG) attached to it [12, 17]. Thus, centrally-generated motor patterns in all the above mentioned preparations revealed intersegmental coupling of activity among CPGs.

Stabilizing effect of the mesothoracic ganglion

Our analysis has revealed that the intrasegmental coupling of the mesothoracic ganglion is stronger than other connections (Fig 12), no matter whether the phase-difference approach (cf. Figs 3, 8, 12 (A) right) or the biased or unbiased DCM approach (cf. Figs 5, 6, 10, 12 (A) left) was used. By cutting the connectives between the meso- and metathoracic ganglia, we could show that the DCM approach was capable of reproducing ”known” coupling strengths in the system. When unspecified changes of connectivity were entered into the model, this resulted in a drastic reduction in intersegmental connectivity strength. As we could not remove any connection from the model without biasing DCM, it still assigned some connectivity strength to the intersegmental connections even though they were not present in the animal. With this we were able to show that even though DCM was developed for neural networks in the human brain, it is still appropriate to be used for less complex systems, i.e. the stick insect thoracic nerve cord. Moreover, this test showed that the presence of the ipsilateral intersegmental meso-meta connection was needed for a strong intrasegmental coupling in the metathoracic ganglion. Our result supports the findings by [28] where the authors showed that phase-coupling of neural activity in the metathoracic ganglion is more stable when the meso- and metathoracic ganglia are interconnected. Here, we found an overall increased meso-meso connectivity after cutting the connectives between the meso- and metathoracic ganglia, while Mantziaris and colleagues [28] observed a slight increase in regularity in meso-meso phase distributions in favor of in phase activity when both (meso- and metathoracic) ganglia were connected. This might be due to the fact, that the DCM approach does not distinguish between in-phase and out-of phase synchronization of the mesothoracic ganglion. Our results suggest that a higher meso-meso coupling is necessary to model the remaining rhythmic behavior after the loss of metathoracic inputs. While meta-meta and pro-pro connections are weaker in the unbiased DCM approach, the lateral intrasegmental meso-meso connectivity remains strong even in the *unbiased*, i.e. randomly selected intervals. In a behavioral study Grabowska et al. could show that stick insects with amputated middle legs display a malfunction of coordination with multiple stepping of front and hind

bioRxiv preprint doi: https://doi.org/10.1101/453423; this version posted February 11, 2019. The copyright holder for this preprint (which was not certified by peer review) is the author/funder. All rights reserved. No reuse allowed without permission.

legs as well as ipsilateral legs being in swing phase simultaneously [18]. Combining these findings, we suggest that the activity of the mesothoracic CPGs stabilizes that of the metathoracic segments, ensuring by that a stable rhythm in the meso- and metathoracic ganglia.

Weak coupling in the prothoracic ganglion

In the DCM approach, the intrasegmental coupling strength of the prothoracic ganglion was the weakest (Fig 12 A, left). In the phase-coupling approach, this connection was amongst the weakest that were analyzed (Fig 12 A, right). It was not significantly weaker than the other connections in the experiments involving pro- and mesothoracic ganglia. However, the meso-meso coupling strength used as a reference here (in pro-meso recordings, gray rectangle), was significantly reduced compared to the meso-meso coupling strength, which served as reference in the meso-meta thoracic recordings (blue rectangle). Thus, adding the prothoracic ganglion to the network to be tested lowered the phase-connectivity in it. A similar effect could be observed in the analysis of the pro-meso-meta ganglia with the DCM approach, where no significant differences between the coupling strengths within the network could be seen, while the reference connection (meso-meso) was significantly reduced compared to that in meso-meta recordings (Fig 12 B). Moreover, when adding the prothoracic ganglion to the network to be analyzed (pro-meso and pro-meso-meta activity), the signal-to-noise ratio decreased, reducing the aforementioned stabilizing effect of the mesothoracic ganglion. These results hint at the special role the front legs have. It has been shown that the front legs can perform additional steps or searching movements independently of other legs [7, 18]. Our results suggest that this might be achieved by a weaker lateral intrasegmental coupling between the prothoracic CPGs and a weaker ipsilateral intersegmental coupling between pro- and mesothoracic CPGs. In the deafferented stick insect preparation, restricted CPG activation in the prothoracic ganglion had indeed no intersegmental effect on the mesothoracic networks [25]. In contrast to this, a recent study by Knebel et al. has reported a strong in phase coupling of pro- and mesothoracic ganglia after restricted activation, i.e. using a split bath preparation, of the prothoracic ganglia in the locust [24]. Furthermore, it has been shown in cockroaches that intrasegmental, i.e. meso-meso activity has a strong anti-phase relationship in the absence of sensory feedback [17]. This is a requirement for producing the tripod coordination pattern, which is preferred by these animals. This behavior is further enhanced by sensory feedback from a single stepping front leg, suggesting an additional stabilizing effect by the prothoracic ganglia. These findings suggest a stronger coupling between pro- and mesothoracic ganglia and less flexibility in front leg movements in locusts and cockroaches.

bioRxiv preprint doi: https://doi.org/10.1101/453423; this version posted February 11, 2019. The copyright holder for this preprint (which was not certified by peer review) is the author/funder. All rights reserved. No reuse allowed without permission.

Coupling from meta- to prothoracic ganglion

The recordings from all three ganglia enabled us to gain insights into the coupling structure involving the pro- and metathoracic ganglia. Our results have revealed an ipsilateral feedback from the meta- to the prothoracic ganglia without any contralateral connection. This result supports the hypothesis used in the model by Daun-Gruhn & Tóth. This hypothesis states that the existence of such a feedback from the hind to the front leg is necessary to establish coordinated locomotor patterns in the three ipsilateral legs [11]. Knebel et al. (2017) could show a clear coupling of pro- and metathoracic ganglia in the case of restricted activation of prothoracic as well as restricted activation of metathoracic ganglia [24]. In contrast to the results presented here, this finding suggests the presence of a bidirectional coupling of both ganglia.

Due to the effects of prothoracic activity on the signal-to-noise ratio in our recordings, it was not possible to predefine intervals of synchronized activity. Furthermore, we found no significant differences in coupling strengths in the case of simultaneous recordings from all three ganglia, while it had previously been shown that depressor activity in all segments seems to be weakly phase coupled in locusts [24].

Comparison with a connectivity model of leg coordination in the cockroach

David and colleagues (2016) reported on CPG coupling strength in the meso- and metathoracic ganglia of the cockroach by calculating the transition latencies and phase relations between bursts of activity [12]. In contrast to the results presented here for the stick insect, ipsilateral connections in the cockroach system were found to be stronger than the contralateral ones, while diagonal coupling interactions were also present in the resulting connectivity scheme reported. Moreover the meso- to metathoracic, descending coupling was weaker than the ascending. Such an asymmetry was not systematically observed in our results. In addition, as reported in [12], intrasegmental metathoracic coupling was stronger than coupling between the mesothoracic hemisegments, whereas the opposite is demonstrated here for the stick insect.

The reasons for these discrepancies between the cockroach and the stick insect systems are not well understood. Importantly, the subesophageal ganglion (SOG) and the abdominal ganglia in the aforementioned study were left attached to the thoracic ganglia. Thus, descending or ascending signals, or both, might affect CPG coordination and coupling strength. Our experiments were performed in the absence of SOG input and we should therefore exercise due care when comparing our results to those of David et al. [12].

In a recent modelling study, Szczecinski et al. [42] demonstrated that interleg coordination patterns in *D. melanogaster* result from the interplay between static stability of the animal and robustness of the coordination pattern. The authors found that at a large variety of walking speeds (hence coordination patterns), only the ipsilateral phase differences change, whereas contralateral phase differences remain

bioRxiv preprint doi: https://doi.org/10.1101/453423; this version posted February 11, 2019. The copyright holder for this preprint (which was not certified by peer review) is the author/funder. All rights reserved. No reuse allowed without permission.

at about 1/2. Their simulation results support this finding. Taking this result into consideration, a stronger ipsilateral coupling can be expected in cockroaches, since they usually exhibit tripod coordination pattern during walking. By contrast, the slow walking stick insects may require weaker ipsilateral coupling that could be affected more strongly by afferent sensory signals. To our knowledge, there is no similar study concerning static stability in other insects. However, it may be that ipsilateral phase relationships are critical for intersegmental leg coordination in other insects as well. It would be interesting to know whether the differences in intra- and intersegmental coupling between stick insects and cockroaches are related to the variable static stability of the two animals in relation to their inherent walking speed.

4 Conclusions

In this paper, we have shown for the first time that well-established methods for analyzing M/EEG data can be adapted for the analysis of pilocarpine-induced fictive locomotor patterns of the stick insect *Carausius morosus* to estimate coupling strength from real data. Applying the DCM approach, we could predict a high probability for the existence of ipsilateral inter- and lateral intrasegmental connections of the CPGs. We could further discern changes in the connectivity of the thoracic ganglia of the stick insect in different experimental conditions. DCM detected the absence of coupling between the meso- and metathoracic ganglia after the connectives had been cut. Using DCM as well as the PC approach, we have established that the intrasegmental mesothoracic connectivity is the strongest from all others in all three thoracic ganglia. Moreover, this coupling has a stabilizing effect on intrasegmental metathoracic activity. Connectivity involving prothoracic ganglia, by contrast, is either weak or depends on the specific network topology to be analyzed. This could account for the fact that the prothoracic ganglia have to allow decoupling of the front legs from the rest of the locomotor system to enable search movements of the front legs independently of the middle and the hind leg movements.

Acknowledgements

We thank Anke Borgmann for useful discussions on the analysis. This study was funded by the University of Cologne Emerging Groups Initiative (CONNECT group) within the framework of the Institutional Strategy of the University of Cologne and the German Excellence Initiative. SD gratefully acknowledges additional support from the German Research Foundation, Germany (DA1953/5-2). CM was an associate member of the RTG 1960 ”Neural Circuit Analysis on the Cellular and Subcellular Level” funded by the DFG.

bioRxiv preprint doi: https://doi.org/10.1101/453423; this version posted February 11, 2019. The copyright holder for this preprint (which was not certified by peer review) is the author/funder. All rights reserved. No reuse allowed without permission.

References

1. Berens, P.: Circstat: a matlab toolbox for circular statistics. J Stat Softw **31**(10), 1–21 (2009)

2. Borgmann, A., Scharstein, H., Büschges, A.: Intersegmental coordination: influence of a single walking leg on the neighboring segments in the stick insect walking system. J. Neurophysiol. **98**(3), 1685–1696 (2007)

3. Büschges, A.: Sensory control and organization of neural networks mediating coordination of multisegmental organs for locomotion. J. Neurophysiol. **93**(3), 1127–1135 (2005)

4. Büschges, A., Akay, T., Gabriel, J.P., Schmidt, J.: Organizing network action for locomotion: insights from studying insect walking. Brain Res Rev **57**(1), 162–171 (2008)

5. Büschges, A., Schmitz, J., Bässler, U.: Rhythmic patterns in the thoracic nerve cord of the stick insect induced by pilocarpine. The Journal of Experimental Biology **198**(2), 435–56 (1995)

6. Chen, C., Henson, R., Stephan, K., Kilner, J., Friston, K.: Forward and backward connections in the brain: a dcm study of functional asymmetries. NeuroImage **45**(2), 453—462 (2009). DOI 10.1016/j.neuroimage.2008.12.041

7. Cruse, H.: The function of the legs in the free walking stick insect, carausius morosus. Journal of Comparative Physiology **112**(2), 235–262 (1976)

8. Cruse, H.: What mechanisms coordinate leg movement in walking arthropods?. Trends in neurosciences **13**(1), 15–21 (1990)

9. Daido, H.: Order function theory of macroscopic phase-locking in globally and weakly coupled limit-cycle oscillators. International Journal of Bifurcation and Chaos **07**(04), 807–829 (1997). DOI 10.1142/S0218127497000601

10. Daun-Gruhn, S., Büschges, A.: From neuron to behavior: dynamic equation-based prediction of biological processes in motor control. Biological cybernetics **105**(1), 71 (2011)

11. Daun-Gruhn, S., Tóth, T.I.: An inter-segmental network model and its use in elucidating gait-switches in the stick insect. Journal of computational neuroscience **31**(1), 43–60 (2011)

12. David, I., Holmes, P., Ayali, A.: Endogenous rhythm and pattern-generating circuit interactions in cockroach motor centres. Biology open pp. bio–018705 (2016)

13. Dean, J.: Leg coordination in the stick insect carausius morosus: effects of cutting thoracic connectives. Journal of Experimental Biology **145**(1), 103–131 (1989)

bioRxiv preprint doi: https://doi.org/10.1101/453423; this version posted February 11, 2019. The copyright holder for this preprint (which was not certified by peer review) is the author/funder. All rights reserved. No reuse allowed without permission.

14. Delcomyn, F.: Neural basis of rhythmic behavior in animals. Science **210**, 492–498 (1980)

15. Foth, E., Bässler, U.: Leg movements of stick insects walking with five legs on a treadwheel and with one leg on a motor-driven belt. I. General results and 1:1-coordination. Biol Cybern **51**(5), 313–318 (1985)

16. Friston, K.J., Bastos, A., Litvak, V., Stephan, K.E., Fries, P., Moran, R.J.: Dcm for complex-valued data: cross-spectra, coherence and phase-delays. Neuroimage **59**(1), 439–455 (2012)

17. Fuchs, E., Holmes, P., Kiemel, T., Ayali, A.: Intersegmental coordination of cockroach locomotion: Adaptive control of centrally coupled pattern generator circuits. Frontiers in Neural Circuits **4**, 125 (2011). DOI 10.3389/fncir.2010.00125

18. Grabowska, M., Godlewska, E., Schmidt, J., Daun-Gruhn, S.: Quadrupedal gaits in hexapod animals–inter-leg coordination in free-walking adult stick insects. Journal of Experimental Biology **215**(24), 4255–4266 (2012)

19. Graham, D., Epstein, S.: Behaviour and motor output for an insect walking on a slippery surface: Ii. backward walking. Journal of experimental biology **118**(1), 287–296 (1985)

20. Grefkes, C., Eickhoff, S.B., Nowak, D.A., Dafotakis, M., Fink, G.R.: Dynamic intra- and interhemispheric interactions during unilateral and bilateral hand movements assessed with fmri and {DCM}. NeuroImage **41**(4), 1382 – 1394 (2008). DOI http://dx.doi.org/10.1016/j.neuroimage.2008.03.048

21. Hess, D., Büschges, A.: Sensorimotor pathways involved in interjoint reflex action of an insect leg. J. Neurobiol. **33**(7), 891–913 (1997)

22. Johnston, R.M., Levine, R.B.: Thoracic leg motoneurons in the isolated cns of adult manduca produce patterned activity in response to pilocarpine, which is distinct from that produced in larvae. Invertebrate Neuroscience **4**(4), 175–192 (2002)

23. Kiebel, S., Garrido, M., Moran, R., Friston, K.: Dynamic causal modelling for eeg and meg. Cognitive Neurodynamics **2**(2), 121–136 (2008). DOI 10.1007/s11571-008-9038-0

24. Knebel, D., Ayali, A., Pflüger, H.J., Rillich, J.: Rigidity and flexibility: the central basis of inter-leg coordination in the locust. Frontiers in neural circuits **10**, 112 (2017)

25. Ludwar, B.C., Göritz, M.L., Schmidt, J.: Intersegmental coordination of walking movements in stick insects. Journal of neurophysiology **93**(3), 1255–1265 (2005)

26. MacQueen, J., et al.: Some methods for classification and analysis of multivariate observations. In: Proceedings of the fifth Berkeley symposium on mathematical statistics and probability, vol. 1, pp. 281–297. Oakland, CA, USA (1967)

bioRxiv preprint doi: https://doi.org/10.1101/453423; this version posted February 11, 2019. The copyright holder for this preprint (which was not certified by peer review) is the author/funder. All rights reserved. No reuse allowed without permission.

27. Mallada, E., Tang, A.: Synchronization of weakly coupled oscillators: coupling, delay and topology. Journal of Physics A: Mathematical and Theoretical **46**(50), 505101 (2013)

28. Mantziaris, C., Bockemühl, T., Holmes, P., Borgmann, A., Daun, S., Büschges, A.: Intra- and intersegmental influences among central pattern generating networks in the walking system of the stick insect. Journal of Neurophysiology **118**(4), 2296–2310 (2017). DOI 10.1152/jn.00321.2017

29. Marder, E., Bucher, D.: Central pattern generators and the control of rhythmic movements. Current Biology **11** (2001). DOI http://dx.doi.org/10.1016/S0960-9822(01)00581-4

30. Marple S.L., J.: Computing the discrete-time ldquo;analytic rdquo; signal via fft. Signal Processing, IEEE Transactions on **47**(9), 2600–2603 (1999). DOI 10.1109/78.782222

31. Moran, R., Kiebel, S., Rombach, N., O'Connor, W., Murphy, K., Reilly, R., Friston, K.: Bayesian estimation of synaptic physiology from the spectral responses of neural masses. NeuroImage **42**(1), 272–284 (2008). DOI 10.1016/j.neuroimage.2008.01.025

32. Moran, R., Kiebel, S., Stephan, K., Reilly, R., Daunizeau, J., Friston, K.: A neural mass model of spectral responses in electrophysiology. NeuroImage **37**(3), 706–720 (2007). DOI 10.1016/j.neuroimage.2007.05.032

33. Moran, R.J., Jung, F., Kumagai, T., Endepols, H., Graf, R., Dolan, R.J., Friston, K.J., Stephan, K.E., Tittgemeyer, M.: Dynamic causal models and physiological inference: A validation study using isoflurane anaesthesia in rodents. PLoS ONE **6**(8), e22790 (2011). DOI 10.1371/journal.pone.0022790

34. Pedregosa, F., Varoquaux, G., Gramfort, A., Michel, V., Thirion, B., Grisel, O., Blondel, M., Prettenhofer, P., Weiss, R., Dubourg, V., Vanderplas, J., Passos, A., Cournapeau, D., Brucher, M., Perrot, M., Duchesnay, E.: Scikit-learn: Machine learning in Python. Journal of Machine Learning Research **12**, 2825–2830 (2011)

35. Penny, W., Litvak, V., Fuentemilla, L., Duzel, E., Friston, K.: Dynamic causal models for phase coupling. Journal of neuroscience methods **183**(1), 19–30 (2009)

36. Rigoux, L., Stephan, K., Friston, K., Daunizeau, J.: Bayesian model selection for group studies – revisited. NeuroImage **84**, 971–985 (2014). DOI 10.1016/j.neuroimage.2013.08.065

37. Rosenblum, M., Pikovsky, A., Kurths, J., Schäfer, C., Tass, P.A.: Phase synchronization: from theory to data analysis. Handbook of biological physics **4**(279-321), 93–94 (2001)

38. Ryckebusch, S., Laurent, G.: Interactions between segmental leg central pattern generators during fictive rhythms in the locust. Journal of neurophysiology **72**(6), 2771–2785 (1994)

bioRxiv preprint doi: https://doi.org/10.1101/453423; this version posted February 11, 2019. The copyright holder for this preprint (which was not certified by peer review) is the author/funder. All rights reserved. No reuse allowed without permission.

39. Schmitz, J.: The depressor trochanteris motoneurones and their role in the coxo-trochanteral feedback loop in the stick insect carausius morosus. Biological cybernetics **55**(1), 25–34 (1986)

40. Schmitz, J., Büschges, A., Delcomyn, F.: An improved electrode design for en passant recording from small nerves. Comparative Biochemistry and Physiology Part A: Physiology **91**(4), 769 – 772 (1988). DOI $10.1016/0300\text{-}9629(88)90963\text{-}2$

41. Sillar, K.T., Clarac, F., Bush, B.M.: Intersegmental coordination of central neural oscillators for rhythmic movements of the walking legs in crayfish, pacifastacus leniusculus. Journal of Experimental Biology **131**(1), 245–264 (1987)

42. Szczecinski, N.S., Bockemuhl, T., Chockley, A.S., Büschges, A.: Static stability predicts the continuum of interleg coordination patterns in drosophila. bioRxiv (2018). DOI $10.1101/374272$

43. Tass, P., Rosenblum, M.G., Weule, J., Kurths, J., Pikovsky, A., Volkmann, J., Schnitzler, A., Freund, H.J.: Detection of $n : m$ phase locking from noisy data: Application to magnetoencephalography. Phys. Rev. Lett. **81**, 3291–3294 (1998). DOI $10.1103/\mathrm{PhysRevLett}.81.3291$

44. Walz, J.M., Goldman, R.I., Carapezza, M., Muraskin, J., Brown, T.R., Sajda, P.: Simultaneous eeg-fmri reveals temporal evolution of coupling between supramodal cortical attention networks and the brainstem. The Journal of Neuroscience **33**(49), 19212–19222 (2013). DOI $10.1523/\mathrm{JNEUROSCI}.2649\text{-}13.2013$

45. Brunner von Wattenwyl, K., Redtenbacher, J.: Die Insektenfamilie der Phasmiden. W. Engelmann, Leipzig (1908)

46. Wendler, G.: The co-ordination of walking movements in arthropods. Symposia of the Society for Experimental Biology **20**, 229–249 (1965)